

Multichannel quantum defect theory with a frame transformation for ultracold molecular collisions in magnetic fields

Masato Morita¹, Paul Brumer¹, and Timur V. Tscherbul²

¹*Chemical Physics Theory Group, Department of Chemistry, and Center for Quantum Information and Quantum Control, University of Toronto, Toronto, Ontario, M5S 3H6, Canada and*

²*Department of Physics, University of Nevada, Reno, Nevada, 89557, USA*

(Dated: September 4, 2023)

We extend the powerful formalism of multichannel quantum defect theory combined with a frame transformation (MQDT-FT) to ultracold molecular collisions in magnetic fields. By solving the coupled-channel equations with hyperfine and Zeeman interactions omitted at short range, MQDT-FT enables a drastically simplified description of the intricate quantum dynamics of ultracold molecular collisions in terms of a small number of short-range parameters. We apply the formalism to ultracold Mg + NH collisions in a magnetic field, achieving a 10^4 -fold reduction in computational effort.

Recent advances in cooling and trapping diatomic and polyatomic molecules have established ultracold molecular gases as an emerging platform for quantum information science, ultracold chemistry, and precision searches for new physics beyond Standard Model [1–4]. The exquisite control over molecular degrees of freedom achieved in these experiments enables the exploration of novel regimes of ultracold chemical dynamics tunable by external electromagnetic fields [5–7]. However, the use of molecules for these applications has been hindered by rapid losses observed in ultracold molecular gases due to the formation of intermediate complexes in two-body collisions [8–15]. Therefore, understanding and controlling ultracold molecular collisions have long been recognized as major goals in the field [1, 3]. This, however, has proven to be an elusive task due to the enormous number of molecular states (rotational, vibrational, fine, and hyperfine) strongly coupled by highly anisotropic interactions and external fields, which results in skyrocketing computational costs of rigorous coupled channel (CC) calculations on ultracold molecular collisions [16, 17]. While efficient basis sets have been developed to mitigate this problem [17–21], fully converged CC calculations including all degrees of freedom are yet to be reported on ultracold K + NaK [22, 23], Na + NaLi [24, 25], and Rb + KRb [14] collisions explored in recent experiments.

A promising avenue toward resolving these difficulties could be based on multichannel quantum defect theory (MQDT), an elegant technique for solving the time-independent Schrödinger equation based on the separation of distance and energy scales in ultracold collisions [26–37]. MQDT allows one to avoid the costly numerical procedure of solving CC equations over extended ranges of the radial coordinate R , collision energy, and magnetic field, leading to a substantial reduction of computational cost [33–40]. However, in conventional MQDT, it is still necessary to solve CC equations in the short-range collision complex region, which is forbiddingly difficult for the atom-molecule systems interacting via deep and strongly anisotropic potentials, such as those studied in recent experiments [14, 22–25].

MQDT becomes especially powerful when combined with a frame transformation (FT) approach, in which the hyperfine-Zeeman structure of colliding atoms is neglected at short range. This results in a large reduction of computational effort and provides a physically meaningful description of ultracold atomic collisions in terms of a few short-range parameters [38–44]. An extension of MQDT-FT to the much more computationally intensive (and less well understood) ultracold molecular collisions would thus be highly desirable. Previous theoretical work has shown that MQDT can be successfully applied to describe ultracold atom-molecule collisions [33–36] and chemical reactions [37], but these calculations did not consider the essential FT aspect of MQDT, which makes it such an indispensable tool in modern ultracold atomic collision theory [38–44].

Here, we show that the MQDT-FT approach can be extended to ultracold molecular collisions in a magnetic field, enabling one to drastically simplify their rigorous theoretical description. This is achieved by using compact CC basis sets at short range, which exclude the hyperfine and Zeeman interactions. These interactions are incorporated at long range via MQDT-FT boundary conditions, resulting in a complete description of ultracold atom-molecule collision dynamics across large collision energy and magnetic field ranges in terms of a small number of short-range parameters. These parameters can be used to, e.g., fit experimental observations and to obtain insight into complex molecular collision dynamics without performing expensive CC calculations. Our results show the potential of MQDT-FT to significantly extend the scope of ultracold atom-molecule collisions and chemical reactions amenable to rigorous quantum dynamical studies, which would facilitate the accurate characterization of atom-molecule Feshbach resonances observed in recent pioneering experiments [22–25], as well as new insights into quantum chaotic behavior and microscopic interactions in atom-molecule collision complexes [45].

Theory. We begin by briefly reviewing the key concepts of MQDT as they apply to ultracold atom-molecule collisions in a magnetic field. The Hamiltonian of the

atom-molecule collision complex is (in atomic units) [46]

$$\hat{H} = -\frac{1}{2\mu R} \frac{\partial^2}{\partial R^2} R + \frac{\hat{l}^2}{2\mu R^2} + \hat{H}_{\text{as}} + \hat{V}(R, \theta). \quad (1)$$

Below we will use ultracold Mg(¹S) + NH($\tilde{X}^3\Sigma^-$) collisions as a representative example, which served as a testbed for applying MQDT to ultracold atom-molecule collisions [33]. We note, however, that our treatment can be readily generalized to collisions of atoms and molecules with a more complex internal structure, and to molecule-molecule collisions. In Eq. (1), μ and \hat{l} are the reduced mass and the orbital angular momentum for the collision, R is the atom-molecule distance, and \hat{H}_{as} is the asymptotic Hamiltonian

$$\hat{H}_{\text{as}} = B_e \hat{\mathbf{N}}^2 + \hat{H}_{\text{fs}} + \hat{H}_{\text{hfs}} + \hat{H}_{\text{Z}}, \quad (2)$$

where B_e is the rotational constant, $\hat{\mathbf{N}}$ is the rotational angular momentum of the molecule, $\hat{H}_{\text{fs}} = \gamma_{\text{sr}} \hat{\mathbf{N}} \cdot \hat{\mathbf{S}} + \frac{2}{3} \lambda_{\text{ss}} \sqrt{\frac{24\pi}{5}} \sum_q (-1)^q Y_{2-q}(\hat{\mathbf{r}}) [\hat{\mathbf{S}} \otimes \hat{\mathbf{S}}]_q^{(2)}$ is the intramolecular fine-structure Hamiltonian, which depends on the electron spin $\hat{\mathbf{S}}$ and the orientation of the molecular axis \mathbf{r} , and γ_{sr} and λ_{ss} are the spin-rotation and spin-spin interaction constants [47, 48]. The Zeeman interaction $\hat{H}_{\text{Z}} = g_S \mu_{\text{B}} \mathbf{B} \cdot \hat{\mathbf{S}}$, where $g_S \simeq 2.002$ is the electron g -factor, μ_{B} is the Bohr magneton, the magnetic field vector \mathbf{B} defines the space-fixed quantization axis z , and the hyperfine interaction \hat{H}_{hfs} is considered below. We use the accurate *ab initio* interaction potential $V(R, \theta)$ for Mg-NH [49], which depends on R and the atom-molecule Jacobi angle θ (see the Supplemental Material for details of CC and MQDT-FT calculations [50]).

In MQDT, the matrix solution Ψ of the Schrödinger equation $\hat{H}\Psi = E\Psi$ in the basis of eigenvectors of the asymptotic Hamiltonian (2) is given by [31, 33]

$$\Psi = R_m^{-1} [\mathbf{f}(R_m) + \mathbf{g}(R_m) \mathbf{K}^{\text{sr}}], \quad (3)$$

where the matching radius $R = R_m$ marks the boundary between the short-range and long-range regions, E is the total energy, \mathbf{K}^{sr} is the short-range K -matrix, which includes open and weakly closed channels, and $\mathbf{f}(R)$ and $\mathbf{g}(R)$ are diagonal matrices of regular and irregular solutions of the one-dimensional radial Schrödinger equations

$$\left[-\frac{1}{2\mu} \frac{\partial^2}{\partial R^2} + U_i^{\text{ref}}(R) \right] \psi_i(R) = E \psi_i(R). \quad (4)$$

Here, $U_i^{\text{ref}}(R) = V_0(R) + l_i(l_i + 1)/(2\mu R^2) + E_i^\infty$ is the MQDT reference potential [33, 50], for the i -th reference channel with threshold energy E_i^∞ and orbital angular momentum l_i , and $V_0(R)$ is the isotropic part of the interaction potential.

Having defined the short-range K -matrix, we take into account the coupling between the open and weakly closed channels by forming the matrix

$$\bar{\mathbf{K}}^{\text{sr}} = \mathbf{K}_{\text{o,o}}^{\text{sr}} - \mathbf{K}_{\text{o,wc}}^{\text{sr}} [\tan \nu + \mathbf{K}_{\text{wc,wc}}^{\text{sr}}]^{-1} \mathbf{K}_{\text{wc,o}}^{\text{sr}}, \quad (5)$$

where $\tan \nu$ is a diagonal matrix with elements $\tan \nu_i$ for weakly closed channels [27, 31, 33]. The zeros of the bound-state phase ($\tan \nu_i = 0$) locate the bound state energy in the i -th reference potential and $\mathbf{K}_{\text{wc,wc}}^{\text{sr}}$ introduces shifts in the resonance positions [31]. We neglect the strongly closed channels, whose coupling with open and weakly closed channels has no effect on scattering dynamics [33, 34, 50]. Here, we define strongly closed channels as those, for which $U_i^{\text{ref}}(R) > E$ for all R [50].

Finally, we take into account the threshold effects using the diagonal matrices of MQDT parameters \mathbf{C} and $\tan \lambda$ for open channels to obtain the $\bar{\mathbf{R}}$ matrix

$$\bar{\mathbf{R}} = \mathbf{C}^{-1} [(\bar{\mathbf{K}}^{\text{sr}})^{-1} - \tan \lambda]^{-1} \mathbf{C}^{-1}, \quad (6)$$

where C_i determines the amplitude of the reference functions and λ_i is the phase difference between the long-range and short-range irregular solutions [32]. Finally, the transition T -matrix may be written as

$$\mathbf{T} = \mathbf{I} - e^{i\xi} [\mathbf{I} + i\bar{\mathbf{R}}] [\mathbf{I} - i\bar{\mathbf{R}}]^{-1} e^{i\xi}, \quad (7)$$

where \mathbf{I} is the unit matrix and ξ is the diagonal matrix of phase shifts ξ_i associated with the energy-normalized reference functions [27, 31–34]. The state-to-state integral cross sections are obtained from the transition probability $|T_{i,f}|^2$ as $\sigma_{i \rightarrow f} = (\pi/k_i^2) |T_{i,f}|^2$, where i and f label the initial and final internal molecular states, $k_i = \sqrt{2\mu E_c}$ is the incident wavevector, and E_c is the collision energy.

In the spirit of MQDT-FT for atomic collisions [38–44], we seek to describe short-range quantum dynamics with a simplified Hamiltonian \hat{H}_0 obtained by omitting the terms, which are small compared to \hat{V} , from \hat{H}_{as} in Eq. (2). To this end, the exact short-range K -matrix (\mathbf{K}^{sr}) corresponding to the original Hamiltonian \hat{H} is obtained from the approximate K -matrix (\mathbf{K}_0^{sr}), which corresponds to the simplified Hamiltonian \hat{H}_0 :

$$\mathbf{K}^{\text{sr}} \simeq \mathbf{U}^\dagger \mathbf{K}_0^{\text{sr}} \mathbf{U}, \quad (8)$$

where \mathbf{U} is the unitary FT matrix composed of the eigenvectors of \hat{H}_{as} in Eq. (2) (see the Supplemental Material [50] for details). Note that \mathbf{K}_0^{sr} is much easier to compute than the exact \mathbf{K}^{sr} because \hat{H}_0 can be chosen in such a way as to exclude the small hyperfine and Zeeman interactions (see below), thus eliminating the need to use enormous CC basis sets including the electron and/or nuclear spin basis functions of the collision partners [21]. In addition, since \hat{H}_0 is independent of external fields, \mathbf{K}_0^{sr} can be efficiently computed using the total angular momentum (TAM) basis as shown below, and it is independent of M , the z projection of J .

Once the FT approximation for \mathbf{K}^{sr} is implemented, the standard MQDT procedure [27, 31–33] can be applied to obtain scattering observables as a function of collision energy and magnetic field. This procedure is computationally efficient, scaling as $O(N)$ with the total number of channels N . The only additional modification is that the threshold energies E_i^∞ should be replaced by exact threshold energies [eigenvalues of \hat{H}_{as} in Eq. (2)].

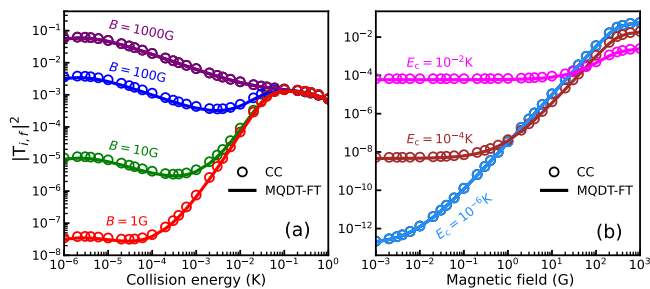


FIG. 1. Probabilities for the spin relaxation transition $M_S = 1$ ($l = 0$) \rightarrow $M'_S = 0$ ($l' = 2$) in cold Mg + ^{14}NH ($N = 0$) collisions plotted as a function of collision energy (a) and magnetic field (b). Solid lines – MQDT-FT calculations, open circles – exact CC results.

We now apply MQDT-FT to describe the quantum dynamics of ultracold Mg + NH collisions in a magnetic field, focusing on the inelastic transitions between the different Zeeman sublevels of NH ($v = 0$, $N = 0$) labeled by the z -projection of the molecule's electron spin $M_S = -1, 0, 1$. These transitions cause trap loss and thus limit the efficiency of sympathetic cooling of NH molecules by Mg atoms [47]. For now, we neglect the hyperfine interaction ($\hat{H}_{\text{as}} = B_e \hat{\mathbf{N}}^2 + \hat{H}_{\text{fs}} + \hat{H}_Z$) and choose the simplified short-range Hamiltonian \hat{H}_0 by neglecting the Zeeman interaction as $\hat{H}_0 = \hat{H} - \hat{H}_Z$. Since \hat{H}_0 is field-independent, we obtain \mathbf{K}_0^{sr} by solving CC equations in the TAM basis $|(NS)jJM\rangle$, where $\hat{\mathbf{J}} = \hat{\mathbf{I}} + \hat{\mathbf{j}}$ is the total angular momentum of the atom-molecule system and $\hat{\mathbf{j}} = \hat{\mathbf{N}} + \hat{\mathbf{S}}$ is that of the diatomic molecule. Because \hat{H}_0 is block diagonal in J and independent of M , the computational cost of MQDT-FT is much smaller than that of conventional MQDT [33].

Figure 1 compares the probabilities $|T_{i \rightarrow f}|^2$ for the spin relaxation transition $M_S = 1 \rightarrow 0$ between the Zeeman levels of NH ($N = 0$) in cold Mg+NH collisions calculated using MQDT-FT with exact CC results. Encouragingly, MQDT-FT provides an essentially exact description of the transition probability as a function of collision energy *and* external magnetic field with only 139 channels as compared to 954 channels required in standard MQDT [34], a 10^3 -fold increase in computational efficiency. The excellent performance of MQDT-FT illustrated in Fig. 1 validates the assumption that \hat{H}_Z plays a negligible role in short-range dynamics. The strong magnetic field dependence of the inelastic probability at 1 μK thus arises entirely from long-range physics. Specifically, inelastic scattering is suppressed by the centrifugal barrier in the outgoing d -wave channel at low magnetic fields [51, 52]. This is an example of physically meaningful insight into ultracold atom-molecule collisions gained from MQDT-FT simulations.

We next address the question of whether MQDT-FT can be used to describe hyperfine interactions, which play a crucial role in ultracold molecular collisions [2, 15], yet are notoriously difficult to describe using standard CC

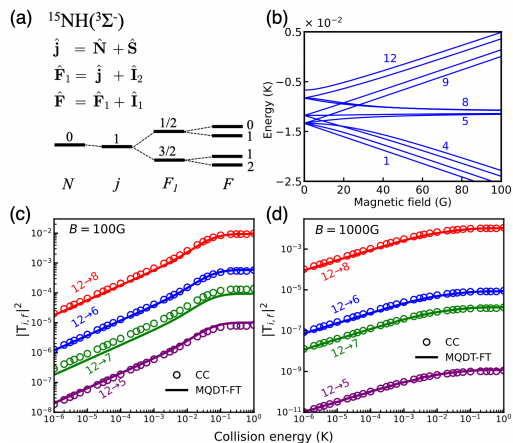


FIG. 2. Hyperfine energy levels of ^{15}NH ($N = 0$) at zero field (a) and as a function of magnetic field (b). State-to-state transition probabilities $|T_{i,l,f,l'}|^2$ plotted as a function of collision energy at $B = 100$ G (c) and $B = 1000$ G (d) for Mg + NH ($N = 0$) collisions for $l = 0$ and $l' = 2$. Solid lines – MQDT-FT results, symbols – exact CC calculations. The initial and final states of NH are indicated next to each curve as $i \rightarrow f$ [see panel (b)].

methods, requiring enormous basis sets [21]. As depicted in Fig. 2(a) the hyperfine structure of ^{15}NH arises from the nuclear spins of ^{15}N ($I_1 = 1/2$) and H ($I_2 = 1/2$) which couple to $\hat{\mathbf{j}}$ (see above) to produce the total angular momentum $\hat{\mathbf{F}}$ of NH, which is a good quantum number at low B -field. The hyperfine structure is described by the Hamiltonian [50, 53, 54]

$$\hat{H}_{\text{hf}} = \sum_{i=1,2} a_i \hat{\mathbf{I}}_i \cdot \hat{\mathbf{S}} + \hat{H}_{\text{ahf}}, \quad (9)$$

where a_i and c_i are the isotropic and anisotropic hyperfine constants for the i -th nucleus, and $\hat{H}_{\text{ahf}} = \sum_i \frac{c_i \sqrt{6}}{3} \sqrt{\frac{4\pi}{5}} \sum_{q=-2}^2 (-1)^q Y_{2-q}(\mathbf{r}) [\hat{\mathbf{I}}_i \otimes \hat{\mathbf{S}}]_q^{(2)}$ is the anisotropic hyperfine interaction. In the high B -field limit, the 12 hyperfine levels of ^{15}NH are arranged in three groups, with 4 states per group, according to the value of $M_S = -1, 0$, and 1, as shown in Fig. 2(b).

To account for the hyperfine structure, we perform MQDT-FT calculations using the same simplified short-range Hamiltonian \hat{H}_0 and the TAM basis set as described above without extra computational costs. It is only necessary to augment \mathbf{K}_0^{sr} by the nuclear spin basis states $|I_1 M_{I_1}\rangle |I_2 M_{I_2}\rangle$ before applying the FT [50].

Figures 2(c) and (d) show transition probabilities between the different hyperfine levels of NH in ultracold collisions with Mg atoms. We observe very good agreement between MQDT-FT and exact CC results, which indicates that the effects of hyperfine structure on ultracold atom-molecule collisions can be accurately described by MQDT-FT. Importantly, only 147 channels need to be coupled in our MQDT-FT calculations, whereas full

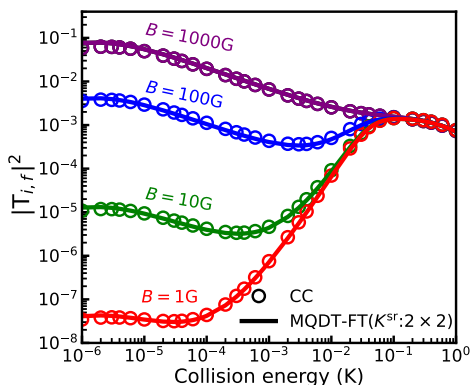


FIG. 3. Probabilities for the transition $M_S = 1, l = 0 \rightarrow M'_S = 0, l' = 2$ in cold $\text{Mg} + {}^{14}\text{NH}(N = 0)$ collisions as a function of collision energy. Solid lines – MQDT-FT results based on a 2×2 short-range K -matrix ($K^{\text{sr}}:2 \times 2$), open circles – exact CC calculations.

CC computations involve as many as 3854 channels [48]. Given the $O(N^3)$ scaling of the computational effort with the number of channels N , MQDT-FT affords a massive reduction of computational cost by a factor of 10^4 .

An attractive feature of the MQDT-FT approach is its capability to describe the complex quantum dynamics of ultracold collisions in terms of a small number of “universal” parameters [39, 40]. While this capability has provided invaluable physical insight into ultracold atomic collisions [39, 40], it has been unclear whether it can be extended to more complex molecular collisions. A minimal MQDT-FT model of ultracold $\text{Mg} + \text{NH}$ collision is based on a 2×2 short-range K -matrix obtained using only the elements of K^{sr} corresponding to the initial and final channels ($K_{ii}^{\text{sr}}, K_{if}^{\text{sr}} = K_{fi}^{\text{sr}}$, and K_{ff}^{sr}).

As shown in Fig. 3, the probability for the $M_S = 1 \rightarrow M'_S = 0$ transition obtained with the two-channel model is in excellent agreement with the full 954-channel results. Remarkably, the quantum dynamics of inelastic spin relaxation in ultracold $\text{Mg} + \text{NH}$ collisions in a magnetic field can be described nearly exactly using just three short-range parameters ($K_{ii}^{\text{sr}}, K_{if}^{\text{sr}}$, and K_{ff}^{sr}) over a wide range of collision energies. This result highlights the universal nature of complex ultracold atom-molecule collisions in a dc magnetic field, and suggests MQDT-FT as a possible alternative to the approaches based on a single-channel universal model (UM) [55, 56]. While the phenomenological y parameter of the UM can be related to the results of CC calculations only in some special cases [56], the MQDT-FT parameters (K_{ij}^{sr}) are readily available from modest CC calculations, which only need to be performed in the short-range region, and do not need to include the Zeeman and hyperfine interactions.

Finally, we consider the possibility of MQDT-FT based on an even more drastically simplified short-range Hamiltonian \hat{H}_0 , which includes only rovibrational degrees of freedom. Because \hat{H}_0 excludes all spin-dependent inter-

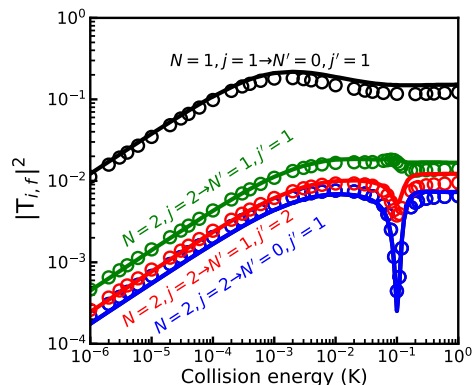


FIG. 4. Collision energy dependence of transition probabilities between the different fine-structure levels of ${}^{14}\text{NH}$ in ultracold collisions with Mg atoms. Symbols – exact CC calculations, lines – MQDT-FT results obtained using the recoupling FT. The quantum numbers for the initial and final states involved in each transition are indicated next to the corresponding curves. All results are for a single incident s -wave component ($l = 0$) and summed over all final l' .

actions, it cannot describe inelastic transitions between the different hyperfine-Zeeman sublevels of $\text{NH}(N = 0)$, which, for collisions with structureless atoms such as Mg , are mediated by intramolecular spin-dependent interactions [46, 52]. We thus focus on inelastic transitions between the different fine-structure components of excited rotational states of NH . We use a modified recoupling technique, which has been successfully applied to such transitions at high collision energies [57–61]. To extend this technique to the ultracold domain, we apply it to the short-range K -matrix rather than the T -matrix, as was done previously [57–61].

Specifically, we obtain K_0^{sr} by solving CC equations for the simplified Hamiltonian $\hat{H}_0 = \hat{H} - \hat{H}_{\text{fs}} - \hat{H}_{\text{hfs}} - \hat{H}_{\text{Z}}$ (see Eqs. (1) and (2)) using the basis set $|(Nl)J_r M_r\rangle$, where $\hat{\mathbf{J}}_r = \hat{\mathbf{N}} + \hat{\mathbf{I}}$ is the total rotational angular momentum of the collision complex [21]. The basis functions $|(Nl)J_r M_r\rangle$ are the eigenstates of \hat{H}_0 in the limit $R \rightarrow \infty$. The eigenstates of $\hat{H}_0 + \hat{H}_{\text{fs}}$ are well approximated by the TAM basis functions $|(NS)j l J M\rangle$ for ${}^{2S+1}\Sigma$ molecules [57] provided the weak spin-spin interaction between the different N states can be neglected. To obtain the desired short-range K -matrix in the $|(NS)j l J M\rangle$ basis from that in the $|(Nl)J_r M_r\rangle$ basis, we use an analytical recoupling transformation [50, 57].

Figure 4 shows that the probabilities for rotationally inelastic fine-structure transitions in ultracold $\text{Mg} + \text{NH}$ collisions are well described by MQDT-FT. Thus, using a spin-independent \hat{H}_0 in short-range CC calculations in the framework of MQDT-FT enables one to describe a wide range of transitions between rotational and fine-structure levels of open-shell molecules in ultracold collisions with atoms.

In summary, we have generalized the powerful MQDT-

FT approach to ultracold atom-molecule collisions in external magnetic fields, providing a robust conceptual and numerical framework for their theoretical description. We have applied the approach to a realistic atom-molecule collision system (Mg + NH) using a variety of short-range Hamiltonians, obtaining encouraging agreement with exact CC calculations in all cases. Our calculations show that MQDT-FT can provide a dramatic (10^4 -fold) reduction of computational effort of CC calculations of atom-molecule collisions compared to standard MQDT [34] due the fact that there is no need to explicitly account for the hyperfine-Zeeman structure of the collision partners at short range. In many cases of practical interest, it will only be necessary to solve CC equations in the strong interaction region employing a rovibrational (TAM) basis in the absence of external fields, which can be efficiently accomplished using currently available computational techniques [36, 45, 62–65]. This opens up the possibility of performing rigorous quantum scattering calculations on a wide array of previously intractable ultracold atom-molecule collisions and chemical reactions in

external fields, including those probed in recent experiments [14, 22–25].

From a conceptual viewpoint, our results show that it is possible to describe the intricate quantum dynamics of ultracold atom-molecule collisions over wide ranges of collision energies and magnetic field in terms of a small number of short-range parameters (three for Mg+NH). This provides a solid basis for the development of few-parameter MQDT-FT models of ultracold atom-molecule (and possibly even molecule-molecule [66]) collisions. Such models, which have been so fruitful in the field of ultracold atomic collisions [39, 40], may allow for novel insights into fascinating quantum dynamics of ultracold molecular collisions.

We thank Chris Greene, John Bohn, James Croft, and Brian Kendrick for stimulating discussions. This work was supported by the NSF CAREER program (PHY-2045681) and by the U.S. AFOSR under Contract FA9550-22-1-0361 to P.B. and T.V.T. Computations were performed on the Niagara supercomputer at the SciNet HPC Consortium.

Supplemental Material

CONTENTS

I. Computational details	6
A. Coupled channel (CC) calculations	6
B. Physical constants	6
C. Interaction potential	6
D. Multi-channel quantum defect theory (MQDT)	6
II. Frame transformation (FT)	7
III. Electron spin transitions	9
IV. Hyperfine transitions	10
V. Short-range K-matrix	10
VI. Fine structure transitions	10
References	11

In this Supplemental Material (SM), we provide technical details of our MQDT-FT calculations as well as some additional results, which complement the figures and discussions in the main text. We describe the computational details in [Section I](#), and present the cross sections for Zeeman and hyperfine transitions in cold Mg+NH($N = 0$) collisions in [Sections III](#) and [IV](#). Results for the short-range K-matrix as a function of collision energy are presented in [Section V](#). In [Section VI](#), the capabilities of the recoupling FT approach to calculate the short-range K-matrix are illustrated by MQDT-FT calculations of fine structure transitions from the $N = 3$, $j = 3$ initial state of NH.

I. COMPUTATIONAL DETAILS

A. Coupled channel (CC) calculations

We performed coupled-channel (CC) calculations to obtain the reference results for cold Mg + NH collisions in a magnetic field, against which we compare our MQDT-FT calculations in the main text. The Hamiltonian of the atom-molecule collision complex is given by Eq. (1) of the main text. We use converged uncoupled basis sets, $|NM_N\rangle|SM_S\rangle|I_1M_{I_1}\rangle|I_2M_{I_2}\rangle|lm_i\rangle$ for Fig. 2 and $|NM_N\rangle|SM_S\rangle|lm_i\rangle$ for Figs. 1 and 3, with $N_{\max} = 6$ and $l_{\max} = 8$ [47]. On the other hand, for Fig. 4, we employ a coupled total angular momentum (TAM) basis set $|l(N_S)jLJM\rangle$ with $N_{\max} = 6$ and $J_{\max} = 5$. The CC equations are solved with the log-derivative propagation method [67] between $R_{\min} = 4a_0$ and $R_{\max} = 500a_0$. We use the propagation interval of $\Delta R = 0.05a_0$ for $R \leq 30a_0$ and $\Delta R = 0.1a_0$ for $R > 30a_0$.

B. Physical constants

We use the same reduced mass of Mg+¹⁴NH ($\mu = 9.232679959$ amu), and spectroscopic constants of ¹⁴NH ($B_e = 16.343$ cm⁻¹, $\gamma_{\text{sr}} = -0.055$ cm⁻¹, and $\lambda_{\text{ss}} = 0.92$ cm⁻¹) as in Refs. [47, 49]. For the calculations shown in Fig. 2 of the main text, we use the reduced mass of $\mu = 9.60046$ amu for Mg+¹⁵NH, the spectroscopic constants of ¹⁵NH ($B_e = 16.2712$ cm⁻¹, $\gamma_{\text{sr}} = -0.0546$ cm⁻¹, and $\lambda_{\text{ss}} = 0.9199$ cm⁻¹), and the hyperfine constants of ¹⁵NH ($b_1 = -1.9406 \times 10^{-3}$ cm⁻¹, $c_1 = 3.1783 \times 10^{-3}$ cm⁻¹, $b_2 = -3.2108 \times 10^{-3}$ cm⁻¹ and $c_2 = 3.0203 \times 10^{-3}$ cm⁻¹) [54].

C. Interaction potential

The interaction potential between Mg (¹S) and NH ($\tilde{X}^3\Sigma^-$) used in our calculations is published as part of the MOLSCAT program suite [49] as pot-Mg_NH.data and vstar-Mg_NH.f. This potential is slightly different from that used in Refs. [33, 47, 48].

D. Multi-channel quantum defect theory (MQDT)

Except for the frame transformation step to obtain the short-range K-matrix (\mathbf{K}^{sr}), the required calculation procedures in MQDT-FT are essentially the same as those of conventional atom-molecule MQDT [33, 34].

The total number of reference channels is $N_{\text{ref}} = N_{\text{o}} + N_{\text{wc}}$ [33], where N_{o} and N_{wc} are the numbers of open and weakly closed channels, respectively. As stated in the main text, we use only weakly closed channels when calculating the short-range K-matrix (i.e., we exclude strongly closed channels as defined in the main text). The value of the matching radius R_m should be determined carefully by exploring the R_m dependence of the results.

We use $R_m = 30a_0$ for all MQDT-FT calculations presented here and in the main text. No sensitivity to R_m was observed in the range $15a_0 \leq R_m \leq 40a_0$ for the results shown in Fig. 1 of the main text and in the range $25a_0 \leq R_m \leq 35a_0$ for those shown in Fig. 2 of the main text.

The reference potentials, $U_i^{\text{ref}}(R)$ ($i = 1, \dots, N_{\text{ref}}$), describe the long-range part of the scattering problem and dissociate into accurate channel energies including Zeeman and/or hyperfine interactions. We employed the isotropic part, $V_0(R)$, of the interaction potential to construct the reference potentials. The reference potentials contain a hard wall at $R = R_{\text{wall}}$ in the short range region ($U_i^{\text{ref}}(R_{\text{wall}}) = +\infty$) restricting the amplitude of the regular reference function at $R = R_{\text{wall}}$. We employ a common wall position $R_{\text{wall}} = 5a_0$ for all reference channels although the final results are not affected by the choice of R_{wall} . We obtain the reference functions for the i -th reference channel by numerically solving the following 1D radial equation [27, 33]

$$\left[\frac{d^2}{dR^2} + K_i^2(R) \right] \psi_i(R) = 0, \quad (1)$$

where $K_i(R) = \sqrt{2\mu[E - U_i^{\text{ref}}(R)]}$ is the local wavevector and E is the total energy. In the following, we refer to the regular solution as $f_i(R)$ ($f_i(R) \rightarrow 0$ as $R \rightarrow 0$) and to the irregular solution as $g_i(R)$. Here, we use the reference potentials with minima at a finite R in the range $0 < R < R_m$ (in Eq. (5) in the main text) and the WKB normalizations are taken at the minimum of the reference potentials following Mies et al. [27].

Once we obtain the values of the regular and irregular reference functions at the matching point ($R = R_m$), we calculate the $N_{\text{ref}} \times N_{\text{ref}}$ short-range K matrix \mathbf{K}_0^{sr} following the matching boundary condition at $R = R_m$:

$$\Psi(R = R_m) = R_m^{-1}[\mathbf{f}(R_m) + \mathbf{g}(R_m)\mathbf{K}_0^{\text{sr}}], \quad (2)$$

where $\mathbf{f}(R_m)$ and $\mathbf{g}(R_m)$ are the diagonal matrices in the asymptotic basis with their diagonal elements given by the values of the reference functions $f_i(R_m)$ and $g_i(R_m)$ [35].

II. FRAME TRANSFORMATION (FT)

Here, as in the main text, \hat{H} denotes the Hamiltonian of the atom-molecule collision complex, and \hat{H}_0 denotes the simplified Hamiltonian used in short-range CC calculations of \mathbf{K}_0 in MQDT-FT. We approximate \mathbf{K}^{sr} by the matrix obtained via the frame transformation (FT) as $\mathbf{K}^{\text{sr}} \simeq \mathbf{U}^\dagger \mathbf{K}_0^{\text{sr}} \mathbf{U}$, where \mathbf{U} is a unitary matrix composed of the eigenstates of the asymptotic Hamiltonian $\hat{H}_{\text{as}} = \lim_{R \rightarrow \infty} \hat{H}$. Since \mathbf{K}_0^{sr} is initially expressed in the basis of eigenstates of the simplified asymptotic Hamiltonian $\hat{H}_{0,\text{as}} = \lim_{R \rightarrow \infty} \hat{H}_0$, it is necessary to establish a relationship between the eigenstates of \hat{H}_{as} and $\hat{H}_{0,\text{as}}$ to represent \mathbf{K}^{sr} in the basis of eigenstates of \hat{H}_{as} .

Once we represent \hat{H}_0 and \hat{H}_{as} in the same basis set, it is straightforward to apply the FT. However, it can be challenging to obtain the eigenvectors of \hat{H}_{as} in the basis set used in short-range CC calculations. The latter are best performed using the TAM basis set, and it is not straightforward to derive and/or implement the matrix elements of \hat{H}_{as} in this basis. To avoid these difficulties, we propose to use the fully uncoupled basis set, in which the matrix elements of \hat{H}_{as} are readily available [46].

For example, to obtain the results shown in Fig. 1 of the main text, the following sequence of steps is used

1. The matrix of \hat{H}_{as} is constructed and diagonalized in the fully uncoupled basis $|NM_N\rangle|SM_S\rangle|lm_l\rangle$. The resulting eigenstates are expressed as linear combinations of the fully uncoupled basis functions

$$|\alpha\rangle = \sum_i c_i^\alpha |i\rangle, \quad (3)$$

where $|i\rangle$ is a short-hand notation for the uncoupled basis functions $|NM_N\rangle|SM_S\rangle|lm_l\rangle$, which includes the quantum numbers N , M_N , M_S , l , and m_l (note that $S = 1$ is conserved), and the expansion coefficients $\{c_i^\alpha\}$ correspond to the α -th eigenvector of \hat{H}_{as} . The calculated eigenvectors are stored for subsequent use in step 4.

2. The CC equations for the simplified Hamiltonian \hat{H}_0 expressed in the primitive TAM basis $|(NS)jJM\rangle$ are integrated numerically out to $R = R_m$. The log-derivative matrix is then transformed from the primitive TAM basis set to the basis of eigenvectors of $\hat{H}_{0,\text{as}}$ to obtain the short-range K matrix $\mathbf{K}_0^{\text{sr},J}$ using the matching condition given by Eq. (2) for each J ($J_{\text{max}} = 5$). Thus, $\mathbf{K}_0^{\text{sr}} = \mathbf{K}_0^{\text{sr},J=0} \oplus \mathbf{K}_0^{\text{sr},J=1} \oplus \dots \oplus \mathbf{K}_0^{\text{sr},J=5}$.
3. For Mg + NH collisions, the eigenstates of $\hat{H}_{0,\text{as}}$ are well approximated by the individual TAM basis functions due to the small spin-spin interaction in NH (in other words, the matrix of $\hat{H}_{0,\text{as}}$ is nearly diagonal in the TAM basis). Therefore, in the following, we assume that \mathbf{K}_0^{sr} is expressed in the TAM basis. If $\hat{H}_{0,\text{as}}$ is not diagonal in this basis, \mathbf{K}^{sr} would need to be transformed to the basis, in which $\hat{H}_{0,\text{as}}$ is diagonal (see the discussion after Step 4).

The matrix elements of \mathbf{K}^{sr} in the basis of eigenstates α and β of \hat{H}_{as} is obtained by applying the FT

$$\langle \alpha | \mathbf{K}^{\text{sr}} | \beta \rangle = \sum_{p,q} d_p^{\alpha*} d_q^\beta \langle p | \mathbf{K}_0^{\text{sr}} | q \rangle, \quad (4)$$

where $|p\rangle$ and $|q\rangle$ are the TAM basis functions, $\{d_p^\alpha\}$ and $\{d_q^\beta\}$ are the eigenvectors of \hat{H}_{as} in the TAM basis. Instead of calculating these eigenvectors directly, we express them via the eigenvectors of \hat{H}_{as} in the fully uncoupled basis (see Step 1) as described below.

4. As noted above, we wish to calculate \mathbf{K}^{sr} in the eigenbasis of \hat{H}_{as} with the latter operator is expressed in the fully uncoupled basis. This is motivated by the ease of evaluating the matrix elements of \hat{H}_{as} in the fully uncoupled basis [46]. It follows from Eq. (3) that

$$\langle \alpha | \mathbf{K}^{\text{sr}} | \beta \rangle = \sum_{i,j} c_i^{\alpha*} c_j^\beta \langle i | \mathbf{K}_0^{\text{sr}} | j \rangle. \quad (5)$$

To express the matrix elements on the right-hand side in terms of the known quantities $\langle p | \mathbf{K}_0^{\text{sr}} | q \rangle$, we use the completeness relation $\hat{1} = \sum_p |p\rangle\langle p|$:

$$\langle \alpha | \mathbf{K}^{\text{sr}} | \beta \rangle = \sum_{i,j} c_i^{\alpha*} c_j^\beta \langle i | \left[\sum_{p,q} |p\rangle\langle p | \mathbf{K}_0^{\text{sr}} | q \rangle \langle q | \right] | j \rangle = \sum_{i,j,p,q} c_i^{\alpha*} c_j^\beta \langle i | p \rangle \langle q | j \rangle \langle p | \mathbf{K}_0^{\text{sr}} | q \rangle, \quad (6)$$

where the overlaps between the fully uncoupled basis state $|i\rangle$ and the TAM basis state $|p\rangle$ are given analytically by Clebsh-Gordan coefficients. We note that the expression in Eq. (6) is more generally applicable to the cases, where the overlaps $\langle i | p \rangle$ are only available from a numerical computation (which could rely on approximations). Additionally, it is not necessary to explicitly construct the matrix \mathbf{K}_0^{sr} in the fully uncoupled basis set in this calculation.

For completeness, we also consider the situation, in which the eigenstates of $\hat{H}_{0,\text{as}}$ are strongly different from the individual TAM basis functions (this is not the case in the present work). In this situation, the assumption discussed in Step 3 above does not hold, and additional summations over the TAM basis functions and the associated overlap coefficients (eigenvectors) appear in Eq. (6). Let $|\phi\rangle$ be an eigenstate of $\hat{H}_{0,\text{as}}$, which is expanded in the TAM basis set as

$$|\phi\rangle = \sum_p h_p^\phi |p\rangle. \quad (7)$$

From Eq. (6), we obtain

$$\langle \alpha | \mathbf{K}^{\text{sr}} | \beta \rangle = \sum_{i,j,\phi,\chi} c_i^{\alpha*} c_j^\beta \langle i | \phi \rangle \langle \chi | j \rangle \langle \phi | \mathbf{K}_0^{\text{sr}} | \chi \rangle. \quad (8)$$

The matrix elements $\langle \phi | \mathbf{K}_0^{\text{sr}} | \chi \rangle$ and the expansion coefficients $\{h_p^\phi\}$ Eq. (7) are available from short-range CC calculations in the TAM basis subject to the matching condition Eq. (2).

The most general FT is then obtained using Eq. (7) as

$$\langle \alpha | \mathbf{K}^{\text{sr}} | \beta \rangle = \sum_{i,j,\phi,\chi} c_i^{\alpha*} c_j^\beta \langle \phi | \mathbf{K}_0^{\text{sr}} | \chi \rangle \sum_{p,q} h_p^\phi h_q^{\chi*} \langle i | p \rangle \langle q | j \rangle. \quad (9)$$

To produce the results shown in Fig. 2 of the main text, we implemented the following sequence of MQDT-FT steps

1. Build and diagonalize the matrix of \hat{H}_{as} (including the hyperfine interactions) in the fully uncoupled basis set $|NM_N\rangle |SM_S\rangle |lm_l\rangle |I_1M_{I_1}\rangle |I_2M_{I_2}\rangle$.
2. This step is the same as Step 2 above. The only difference is that the number of J -blocks is increased to $J_{\text{max}} = 7$.
3. As in Step 3 above, we assume that the individual TAM basis functions $|(NS)jLJM\rangle$ are the eigenstates of $\hat{H}_{0,\text{as}}$. In this case, \hat{H}_{as} includes the nuclear spin degrees of freedom for the two nuclei of NH but $\hat{H}_{0,\text{as}}$ is identical to that used above (see the steps for Fig. 1).

Because the short-range K -matrix is computed with the nuclear spin degrees of freedom omitted, we need to reintroduce them before applying MQDT boundary conditions (which do include the nuclear spin degrees of freedom). To this end, we augment $\mathbf{K}_0^{\text{sr}} \rightarrow \mathbf{K}_0^{\text{sr}} \otimes \mathbf{I}$, where \mathbf{I} is a 4×4 unit matrix in the basis of 4 possible nuclear spin states of ^{15}NH , $|M_{I_1} = \pm 1/2, M_{I_2} = \pm 1/2\rangle$. The new basis for $\mathbf{K}_0^{\text{sr}} \otimes \mathbf{I}$ is given by the direct product of the TAM basis and $|I_1M_{I_1}\rangle |I_2M_{I_2}\rangle$, namely $|(NS)jLJM\rangle |I_1M_{I_1}\rangle |I_2M_{I_2}\rangle$.

4. Finally, we identify $|i\rangle \leftrightarrow |NM_N\rangle |SM_S\rangle |lm_l\rangle |I_1M_{I_1}\rangle |I_2M_{I_2}\rangle$ and $|p\rangle \leftrightarrow |(NS)jLJM\rangle |I_1M_{I_1}\rangle |I_2M_{I_2}\rangle$ and use Eq. (6) to obtain the desired matrix elements of \mathbf{K}^{sr} in the basis of eigenstates of \hat{H}_{as} .

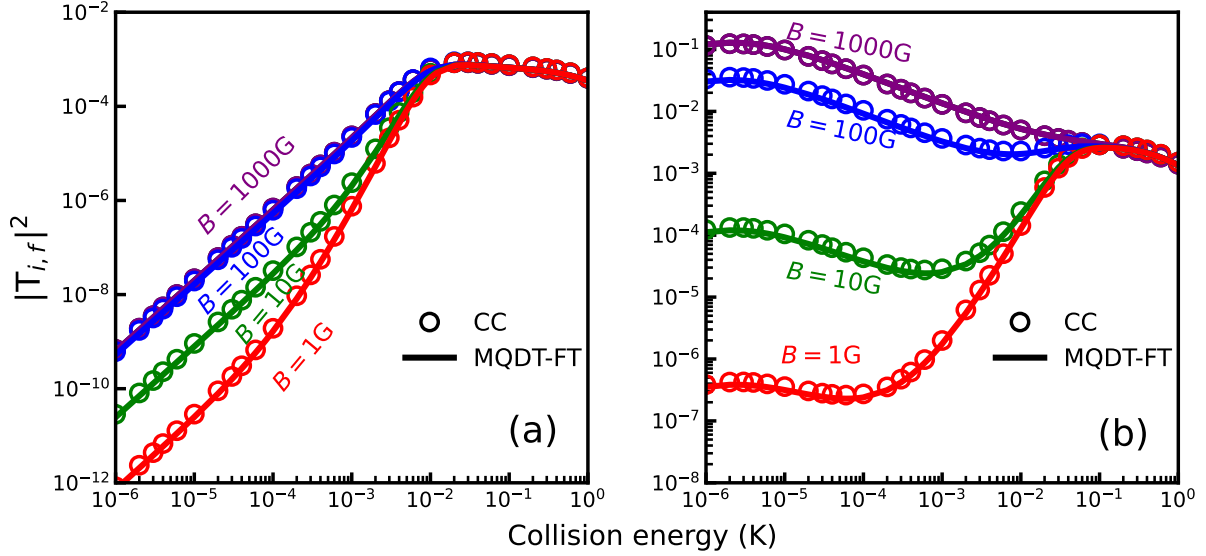


FIG. 1. Probabilities for the spin relaxation transitions (a) $M_S = 1$ ($l = 1$) \rightarrow $M'_S = 0$ ($l' = 1$) and (b) $M_S = 1$ ($l = 0$) \rightarrow $M'_S = -1$ ($l' = 2$) in $\text{Mg} + {}^{14}\text{NH}$ ($N = 0$) collisions. Open circles – exact CC calculations, solid lines – MQDT-FT results. The magnitude of the external magnetic field is indicated next to each curve.

III. ELECTRON SPIN TRANSITIONS

To further illustrate the good agreement between our MQDT-FT results and exact CC calculations (see Fig. 1 of the main text), we show in Fig. 1 a sampling of state-to-state transitions in ultracold $\text{Mg} + \text{NH}$ collisions. While our main interest here is in ultracold s -wave collisions, we also show the results for the $M_S = 1$ ($l = 1$) \rightarrow $M'_S = 0$ ($l' = 1$) transition in panel (a) to demonstrate the capability of MQDT-FT to describe p -wave collisions. In panel (b), we

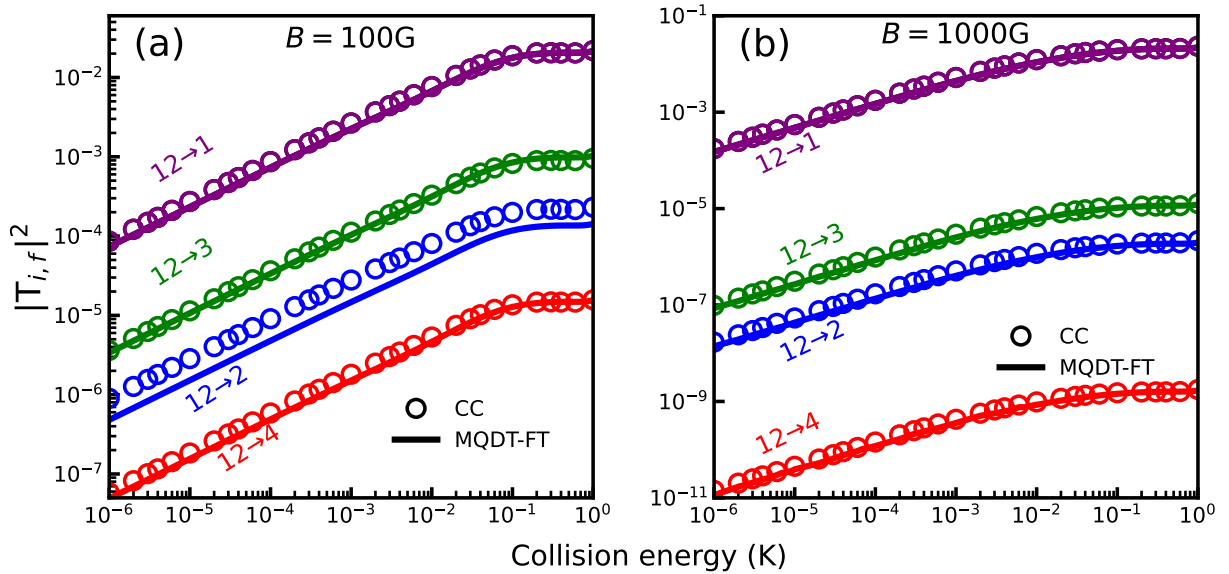


FIG. 2. Probabilities for the state-to-state transitions ($l = 0 \rightarrow l' = 2$) at the magnetic field of (a) $B = 100\text{G}$ (b) $B = 1000\text{G}$ in $\text{Mg} + {}^{15}\text{NH}$ ($N = 0$) collisions. Open circles – exact CC calculations, solid lines – MQDT-FT results. The initial and final states of ${}^{15}\text{NH}$ ($N = 0$) are indicated next to each curve.

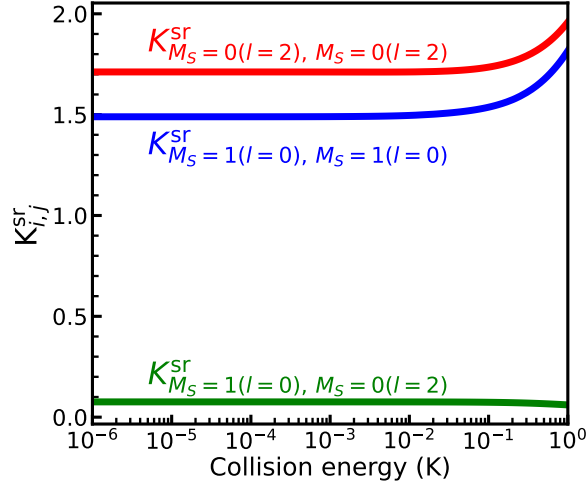


FIG. 3. Elements of the 2×2 short-range K -matrix plotted as functions of collision energy at $B = 1000$ G for the spin relaxation transition $M_S = 1$ ($l = 0$) \rightarrow $M'_S = 0$ ($l' = 2$) in $\text{Mg} + {}^{14}\text{NH}$ ($N = 0$) collisions.

show the results for the $M_S = 1$ ($l = 0$) \rightarrow $M'_S = -1$ ($l' = 2$) transition, which is similar to the $M_S = 1$ ($l = 0$) \rightarrow $M'_S = 0$ ($l' = 2$) transition (see Fig. 1 of the main text).

IV. HYPERFINE TRANSITIONS

In Fig. 2, we show the cross sections for the hyperfine transitions to the final states of ${}^{15}\text{NH}$ ($N = 0$) corresponding to $M'_S = -1$ (see the main text) in s -wave collisions of Mg atoms with ${}^{15}\text{NH}$ molecules initially in the highest energy state (12). We observe excellent agreement between MQDT-FT and exact CC results for most transitions. The agreement improves at higher magnetic fields.

V. SHORT-RANGE K-MATRIX

In Fig. 3 of the main text, we show MQDT-FT results for spin relaxation cross sections in $\text{Mg} + \text{NH}$ collisions obtained using a reduced 2×2 short-range K -matrix. Figure 3 shows the variation of the matrix elements K_{ij}^{sr} with collision energy. Both diagonal (blue and red) and off-diagonal (green) elements are constant throughout the low energy region ($E_c < 10\text{mK}$), indicating that 3 parameters are sufficient to describe spin relaxation in cold $\text{Mg} + \text{NH}$ collisions over a wide range of collision energies spanning 4 orders of magnitude.

We also observed no magnetic field dependence of K_{ij}^{sr} . In particular, the off-diagonal matrix element $K_{M_S=1(l=0), M_S=0(l=2)}^{\text{sr}}$ is conserved to within 6 significant digits in the $B = 1 - 1000$ G range at $E_c = 10^{-6}\text{K}$.

VI. FINE STRUCTURE TRANSITIONS

To calculate the cross sections for fine-structure transitions via the MQDT-FT procedure outlined in the main text, it is necessary to express the short-range K -matrix in the $|(NS)j_lJM\rangle$ basis. However, our short-range K -matrix is defined in the spin-free $|(Nl)J_rM_r\rangle$ basis. These basis sets are related by an analytical recoupling transformation given by Eq. (2.27) of Ref. [57]

$$K_{N'S'j'l', NSj_l}^{\text{sr}, J} = \sum_{J_r=|N-l|}^{N+l} [J_r][j'l']^{1/2} (-1)^{-l'+l+j'-j} \begin{Bmatrix} S & N' & j' \\ l' & J & J_r \end{Bmatrix} \begin{Bmatrix} S & N & j \\ l & J & J_r \end{Bmatrix} K_{0, N'l', Nl}^{\text{sr}, J_r}, \quad (10)$$

where $\{\}$ denotes a 6- j symbol, $[J_r] = (2J_r + 1)$, and $[j, j'] = (2j + 1)(2j' + 1)$.

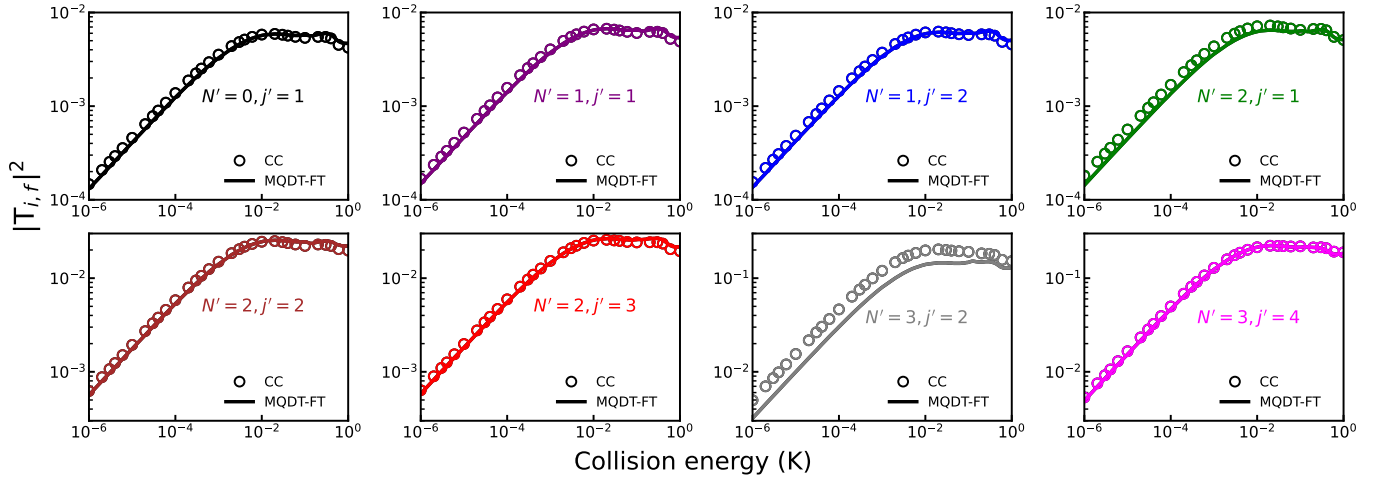


FIG. 4. Fine structure transition probabilities in ultracold $\text{Mg} + {}^{14}\text{NH}(N = 3, j = 3)$ collisions plotted as functions of collision energy for all possible final states and $l = 0$.

In Fig. 4(b) of the main text, we show the cross sections for fine structure transitions from the $N = 3, j = 3$ ($l = 0$) initial state of NH in cold collisions with Mg atoms. Figure 4 shows an extended sample of the results for all possible final states of NH using the recoupling FT technique (see the main text). All the transitions accompanied by rotational de-excitation ($N = 3 \rightarrow N' = 0, 1, \text{ and } 2$) are seen to be accurately described by MQDT-FT. For the N -conserving, j -changing transitions within the $N = 3$ manifold, we observe a slight discrepancy between the CC and MQDT results for $j' = 2$. The overall collision energy dependence of this transition is well reproduced by MQDT-FT. This can be explained by noting that the recoupling transformation (Eq. (10) of the main text) relies on the electron spin playing a spectator role and neglects the intramolecular spin-spin interaction in NH, which plays an important role in N -conserving fine structure transitions.

-
- [1] L. D. Carr, D. DeMille, R. V. Krems, and J. Ye, Cold and ultracold molecules: science, technology and applications, *New. J. Phys.* **11**, 055049 (2009).
 - [2] N. Balakrishnan, Perspective: Ultracold molecules and the dawn of cold controlled chemistry, *J. Chem. Phys.* **145**, 150901 (2016).
 - [3] J. L. Bohn, A. M. Rey, and J. Ye, Cold molecules: Progress in quantum engineering of chemistry and quantum matter, *Science* **357**, 1002 (2017).
 - [4] D. DeMille, J. M. Doyle, and A. O. Sushkov, Probing the frontiers of particle physics with tabletop-scale experiments, *Science* **357**, 990 (2017).
 - [5] M. Lemeshko, R. V. Krems, J. M. Doyle, and S. Kais, Manipulation of molecules with electromagnetic fields, *Mol. Phys.* **111**, 1648 (2013).
 - [6] R. Krems, B. Friedrich, and W. Stwalley, *Cold Molecules: Theory, Experiment, Applications (1st ed.)* (CRC Press., 2009).
 - [7] O. Dulieu and A. Osterwalder, *Cold Chemistry: Molecular Scattering and Reactivity Near Absolute Zero* (The Royal Society of Chemistry, 2017).
 - [8] M. Mayle, B. P. Ruzic, and J. L. Bohn, Statistical aspects of ultracold resonant scattering, *Phys. Rev. A* **85**, 062712 (2012).
 - [9] M. Mayle, G. Quémener, B. P. Ruzic, and J. L. Bohn, Scattering of ultracold molecules in the highly resonant regime, *Phys. Rev. A* **87**, 012709 (2013).
 - [10] A. Christianen, M. W. Zwierlein, G. C. Groenenboom, and T. Karman, Photoinduced Two-Body Loss of Ultracold Molecules, *Phys. Rev. Lett.* **123**, 123402 (2019).
 - [11] P. D. Gregory, M. D. Frye, J. A. Blackmore, E. M. Bridge, R. Sawant, J. M. Hutson, and S. L. Cornish, Sticky collisions of ultracold RbCs molecules, *Nat. Commun.* **10**, 3104 (2019).
 - [12] Y. Liu, M.-G. Hu, M. A. Nichols, D. D. Grimes, T. Karman, H. Guo, and K.-K. Ni, Photo-excitation of long-lived transient intermediates in ultracold reactions, *Nat. Phys.* **16**, 1132 (2020).
 - [13] P. Gersema, K. K. Voges, M. Meyer zum Alten Borgloh, L. Koch, T. Hartmann, A. Zenesini, S. Ospelkaus, J. Lin, J. He, and D. Wang, Probing Photoinduced Two-Body Loss of Ultracold Nonreactive Bosonic ${}^{23}\text{Na}{}^{87}\text{Rb}$ and ${}^{23}\text{Na}{}^{39}\text{K}$ Molecules, *Phys. Rev. Lett.* **127**, 163401 (2021).
 - [14] M. A. Nichols, Y.-X. Liu, L. Zhu, M.-G. Hu, Y. Liu, and K.-K. Ni, Detection of Long-Lived Complexes in Ultracold

Atom-Molecule Collisions, *Phys. Rev. X* **12**, 011049 (2022).

- [15] R. Bause, A. Christianen, A. Schindewolf, I. Bloch, and X.-Y. Luo, Ultracold Sticky Collisions: Theoretical and Experimental Status, *J. Phys. Chem. A* **127**, 729 (2023).
- [16] M. Morita, R. V. Krems, and T. V. Tscherbul, Universal probability distributions of scattering observables in ultracold molecular collisions, *Phys. Rev. Lett.* **123**, 013401 (2019).
- [17] M. Morita, J. Klos, and T. V. Tscherbul, Full-dimensional quantum scattering calculations on ultracold atom-molecule collisions in magnetic fields: The role of molecular vibrations, *Phys. Rev. Res.* **2**, 043294 (2020).
- [18] T. V. Tscherbul and A. Dalgarno, Quantum theory of molecular collisions in a magnetic field: Efficient calculations based on the total angular momentum representation, *J. Chem. Phys.* **133** (2010).
- [19] Y. V. Suleimanov, T. V. Tscherbul, and R. V. Krems, Efficient method for quantum calculations of molecule-molecule scattering properties in a magnetic field, *J. Chem. Phys.* **137** (2012).
- [20] M. Morita, M. B. Kosicki, P. S. Żuchowski, and T. V. Tscherbul, Atom-molecule collisions, spin relaxation, and sympathetic cooling in an ultracold spin-polarized $\text{Rb}(^2\text{S}) - \text{SrF}(^2\Sigma^+)$ mixture, *Phys. Rev. A* **98**, 042702 (2018).
- [21] T. V. Tscherbul and J. P. D’Incao, Ultracold molecular collisions in magnetic fields: Efficient incorporation of hyperfine structure in the total rotational angular momentum representation, [arXiv:2306.05563](https://arxiv.org/abs/2306.05563).
- [22] H. Yang, D.-C. Zhang, L. Liu, Y.-X. Liu, J. Nan, B. Zhao, and J.-W. Pan, Observation of magnetically tunable Feshbach resonances in ultracold $^{23}\text{Na}^{40}\text{K} + ^{40}\text{K}$ collisions, *Science* **363**, 261 (2019).
- [23] X.-Y. Wang, M. D. Frye, Z. Su, J. Cao, L. Liu, D.-C. Zhang, H. Yang, J. M. Hutson, B. Zhao, C.-L. Bai, and J.-W. Pan, Magnetic Feshbach resonances in collisions of $^{23}\text{Na}^{40}\text{K}$ with ^{40}K , *New J. Phys.* **23**, 115010 (2021).
- [24] H. Son, J. J. Park, Y.-K. Lu, A. O. Jamison, T. Karman, and W. Ketterle, Control of reactive collisions by quantum interference, *Science* **375**, 1006 (2022).
- [25] J. J. Park, H. Son, Y.-K. Lu, T. Karman, M. Gronowski, M. Tomza, A. O. Jamison, and W. Ketterle, Spectrum of feshbach resonances in $\text{NaLi} + \text{Na}$ collisions, *Phys. Rev. X* **13**, 031018 (2023).
- [26] C. H. Greene, A. R. P. Rau, and U. Fano, General form of the quantum-defect theory. II, *Phys. Rev. A* **26**, 2441 (1982).
- [27] F. H. Mies, A multichannel quantum defect analysis of diatomic predissociation and inelastic atomic scattering, *J. Chem. Phys.* **80**, 2514 (1984).
- [28] B. Gao, Theory of slow-atom collisions, *Phys. Rev. A* **54**, 2022 (1996).
- [29] B. Gao, Analytic description of atomic interaction at ultracold temperatures: The case of a single channel, *Phys. Rev. A* **80**, 012702 (2009).
- [30] B. Gao, Analytic description of atomic interaction at ultracold temperatures. II. Scattering around a magnetic Feshbach resonance, *Phys. Rev. A* **84**, 022706 (2011).
- [31] F. H. Mies and M. Raoult, Analysis of threshold effects in ultracold atomic collisions, *Phys. Rev. A* **62**, 012708 (2000).
- [32] M. Raoult and F. H. Mies, Feshbach resonance in atomic binary collisions in the Wigner threshold law regime, *Phys. Rev. A* **70**, 012710 (2004).
- [33] J. F. E. Croft, A. O. G. Wallis, J. M. Hutson, and P. S. Julienne, Multichannel quantum defect theory for cold molecular collisions, *Phys. Rev. A* **84**, 042703 (2011).
- [34] J. F. E. Croft, J. M. Hutson, and P. S. Julienne, Optimized multichannel quantum defect theory for cold molecular collisions, *Phys. Rev. A* **86**, 022711 (2012).
- [35] J. F. E. Croft and J. M. Hutson, Multichannel quantum defect theory for cold molecular collisions with a strongly anisotropic potential energy surface, *Phys. Rev. A* **87**, 032710 (2013).
- [36] J. Hazra, B. P. Ruzic, N. Balakrishnan, and J. L. Bohn, Multichannel quantum defect theory for rovibrational transitions in ultracold molecule-molecule collisions, *Phys. Rev. A* **90**, 032711 (2014).
- [37] J. Hazra, B. P. Ruzic, J. L. Bohn, and N. Balakrishnan, Quantum defect theory for cold chemistry with product-quantum-state resolution, *Phys. Rev. A* **90**, 062703 (2014).
- [38] J. P. Burke, C. H. Greene, and J. L. Bohn, Multichannel cold collisions: Simple dependences on energy and magnetic field, *Phys. Rev. Lett.* **81**, 3355 (1998).
- [39] J. P. Burke and J. L. Bohn, Ultracold scattering properties of the short-lived Rb isotopes, *Phys. Rev. A* **59**, 1303 (1999).
- [40] B. Gao, E. Tiesinga, C. J. Williams, and P. S. Julienne, Multichannel quantum-defect theory for slow atomic collisions, *Phys. Rev. A* **72**, 042719 (2005).
- [41] T. M. Hanna, E. Tiesinga, and P. S. Julienne, Prediction of Feshbach resonances from three input parameters, *Phys. Rev. A* **79**, 040701 (2009).
- [42] Z. Idziaszek, A. Simoni, T. Calarco, and P. S. Julienne, Multichannel quantum-defect theory for ultracold atom-ion collisions, *New. J. Phys.* **13**, 083005 (2011).
- [43] J. Pérez-Ríos, S. Dutta, Y. P. Chen, and C. H. Greene, Quantum defect theory description of weakly bound levels and Feshbach resonances in LiRb, *New. J. Phys.* **17**, 045021 (2015).
- [44] J.-L. Li, X.-J. Hu, G.-R. Wang, Y.-C. Han, and S.-L. Cong, Simple model for predicting and analyzing magnetically induced Feshbach resonances, *Phys. Rev. A* **91**, 042708 (2015).
- [45] J. F. E. Croft, C. Makrides, M. Li, A. Petrov, B. K. Kendrick, N. Balakrishnan, and S. Kotochigova, Universality and chaoticity in ultracold $\text{K} + \text{KRb}$ chemical reactions, *Nat. Commun.* **8**, 15897 (2017).
- [46] R. V. Krems and A. Dalgarno, Quantum-mechanical theory of atom-molecule and molecular collisions in a magnetic field: Spin depolarization, *J. Chem. Phys.* **120**, 2296 (2004).
- [47] A. O. G. Wallis and J. M. Hutson, Production of ultracold NH molecules by sympathetic cooling with Mg, *Phys. Rev. Lett.* **103**, 183201 (2009).

- [48] M. L. González-Martínez and J. M. Hutson, Effect of hyperfine interactions on ultracold molecular collisions: $\text{NH}(^3\Sigma^-)$ with $\text{Mg}(^1\text{S})$ in magnetic fields, *Phys. Rev. A* **84**, 052706 (2011).
- [49] J. M. Hutson and C. R. Le Sueur, MOLSCAT: A program for non-reactive quantum scattering calculations on atomic and molecular collisions, *Comput. Phys. Commun.* **241**, 9 (2019).
- [50] See Supplemental Material at [URL] for details of MQDT-FT calculations.
- [51] A. Volpi and J. L. Bohn, Magnetic-field effects in ultracold molecular collisions, *Phys. Rev. A* **65**, 052712 (2002).
- [52] W. C. Campbell, T. V. Tscherbul, H.-I. Lu, E. Tsikata, R. V. Krems, and J. M. Doyle, Mechanism of Collisional Spin Relaxation in $^3\Sigma$ Molecules, *Phys. Rev. Lett.* **102**, 013003 (2009).
- [53] Bailleux, S., Martin-Drumel, M. A., Margulès, L., Pirali, O., Włodarczak, G., Roy, P., Roueff, E., Gerin, M., Faure, A., and Hily-Blant, P., High-resolution terahertz spectroscopy of the ^{15}NH radical ($\tilde{X}^3\Sigma^-$), *A&A* **538**, A135 (2012).
- [54] L. Bizzocchi, M. Melosso, L. Dore, C. D. Esposti, F. Tamassia, D. Prudenzi, V. Lattanzi, J. Laas, S. Spezzano, B. M. Giuliano, C. P. Endres, and P. Caselli, Accurate Laboratory Measurement of the Complete Fine Structure of the $N = 1 - 0$ Transition of ^{15}NH , *Astrophys. J.* **863**, 3 (2018).
- [55] Z. Idziaszek and P. S. Julienne, Universal Rate Constants for Reactive Collisions of Ultracold Molecules, *Phys. Rev. Lett.* **104**, 113202 (2010).
- [56] M. D. Frye, P. S. Julienne, and J. M. Hutson, Cold atomic and molecular collisions: approaching the universal loss regime, *New J. Phys.* **17**, 045019 (2015).
- [57] G. C. Corey and F. R. McCourt, Inelastic differential and integral cross sections for $^{2S+1}\Sigma$ linear molecule- ^1S atom scattering: the use of Hund's case (b) representation, *J. Phys. Chem.* **87**, 2723 (1983).
- [58] M. H. Alexander and P. J. Dagdigan, Collision-induced transitions between molecular hyperfine levels: Quantum formalism, propensity rules, and experimental study of $\text{CaBr}(X^2\Sigma^+) + \text{Ar}$, *J. Chem. Phys.* **83**, 2191 (1985).
- [59] G. C. Corey, M. H. Alexander, and J. Schaefer, Quantum studies of inelastic collisions of $\text{O}_2(X^3\Sigma_g^-)$ with He: Polarization effects and collisional propensity rules, *J. Chem. Phys.* **85**, 2726 (1986).
- [60] F. Lique and J. Klos, Hyperfine excitation of CN by He, *Mon. Not. R. Astron. Soc.: Lett.* **413**, L20 (2011).
- [61] Marinakis, S., Kalugina, Y., Klos, J., and Lique, F., Hyperfine excitation of CH and OH radicals by He, *A&A* **629**, A130 (2019).
- [62] D. Skouteris, J. Castillo, and D. Manolopoulos, ABC: a quantum reactive scattering program, *Comput. Phys. Commun.* **133**, 128 (2000).
- [63] R. T. Pack and G. A. Parker, Quantum reactive scattering in three dimensions using hyperspherical (APH) coordinates. Theory, *J. Chem. Phys.* **87**, 3888 (1987).
- [64] B. K. Kendrick, Non-adiabatic quantum reactive scattering in hyperspherical coordinates, *J. Chem. Phys.* **148**, 044116 (2018).
- [65] M. Morita, B. K. Kendrick, J. Klos, S. Kotochigova, P. Brumer, and T. V. Tscherbul, Signatures of Non-universal Quantum Dynamics of Ultracold Chemical Reactions of Polar Alkali Dimer Molecules with Alkali Metal Atoms: $\text{Li}(^2\text{S}) + \text{NaLi}(a^3\Sigma^+) \rightarrow \text{Na}(^2\text{S}) + \text{Li}_2(a^3\Sigma_u^+)$, *J. Phys. Chem. Lett.* **14**, 3413 (2023).
- [66] J. J. Park, Y.-K. Lu, A. O. Jamison, T. V. Tscherbul, and W. Ketterle, A Feshbach resonance in collisions between triplet ground-state molecules, *Nature* **614**, 54 (2023).
- [67] B. Johnson, The multichannel log-derivative method for scattering calculations, *J. Comput. Phys.* **13**, 445 (1973).